

# First-order variance of travel time in nonstationary formations

Olaf A. Cirpka and Wolfgang Nowak

Institut für Wasserbau, Universität Stuttgart, Stuttgart, Germany

Received 5 November 2003; revised 19 January 2004; accepted 22 January 2004; published 10 March 2004.

[1] Evaluating uncertainty in solute transport under nonstationary flow conditions is a computationally demanding task. This is particularly true for cases with a two-point covariance function of log conductivity depending on the actual positions of the points rather than their distance vector. These may occur when the geological formation exhibits a trend. Nonstationarity can also be the result of uncertainty in the trend parameters of the mean log conductivity value, or it may originate from conditioning of the log conductivity field to measurements of, for example, head or conductivity. We present an efficient numerical method for evaluating the variance of travel time in such formations. We cover cases in which the nonstationary covariance functions are constructed from stationary counterparts, either by scaling functions or by summation with nonstationary functions resulting from marginalization or conditioning. We apply a matrix-based first-order second-moment (FOSM) method for uncertainty propagation, using the continuous adjoint-state method for coupled systems to evaluate the sensitivity matrix. The resulting matrix-matrix multiplications are accelerated by fast Fourier transformation (FFT) techniques after periodic embedding of the covariance matrices referring to the stationary counterparts. The combination of these methods makes it possible to compute the travel time uncertainty in domains discretized by several hundred thousand log conductivity values on standard personal computers within a reasonable time-frame. For demonstration, we apply the method to a binary medium and a medium exhibiting a continuous trend in the covariance function. In the latter application we also demonstrate the effects of marginalization and conditioning. *INDEX TERMS*: 1829 Hydrology: Groundwater hydrology; 1869 Hydrology: Stochastic processes; 1832 Hydrology: Groundwater transport; *KEYWORDS*: adjoint-state method, first-order second-moment method, nonstationarity, periodic embedding, travel time

**Citation:** Cirpka, O. A., and W. Nowak (2004), First-order variance of travel time in nonstationary formations, *Water Resour. Res.*, 40, W03507, doi:10.1029/2003WR002851.

## 1. Introduction

[2] Over the past two decades, stochastic theory has been proven useful in dealing with heterogeneity and uncertainty in natural porous formations. In the geostatistical framework, the hydraulic conductivity and other properties of the formation are treated as random space variables characterized by their statistical moments. From these, one may derive the statistical moments of dependent quantities such as heads, velocities, and concentrations. A common measure of uncertainty in solute transport is the variance of travel time, i.e., the time it takes for a solute particle to be transported from the release point to an observation plane [Shapiro and Cvetkovic, 1988; Dagan et al., 1992]. The travel time is also given by the first temporal moment of a concentration breakthrough curve normalized by its zeroth moment [Harvey and Gorelick, 1995]. Together with the variance of lateral displacement, the travel time variance has been used in solute-flux approaches to macrodispersion in heterogeneous formations [see Rubin, 2003, chap. 9–10].

[3] Closed-form and semi-analytical expressions of travel time statistics exist for stationary velocity fields [Shapiro and Cvetkovic, 1988; Cvetkovic et al., 1992]. The latter

require stationarity of the underlying (log)conductivity field, an unbounded domain, and a uniform mean hydraulic gradient. Accounting for realistic boundary conditions in the flow problem leads to nonstationarity in the velocity field even when the log conductivity field is stationary. Some studies on nonstationary flow consider boundary conditions as the only cause of nonstationarity [Rubin and Bellin, 1994; Fiori et al., 1998]. Others allow for a nonuniform expected value of the log conductivity but require its covariance function to be invariant with respect to translation [Li and McLaughlin, 1995; Indelman and Rubin, 1995]. The most general case also includes nonstationarity in the covariance function of the log conductivity field [Zhang, 1998]. In the present study, we consider numerical methods for uncertainty propagation in media with a nonstationary log conductivity covariance function. Nonstationarity due to boundary conditions is implicitly included.

[4] Zhang et al. [2000] analyzed moments of travel time and lateral displacement in nonstationary flow using a Lagrangian approach in which they integrated the velocity covariance, plus two correction terms accounting for spatial trends in mean flow, along the mean trajectory. The nonstationary covariance function of the velocity field was evaluated by the numerical method of moments introduced by Zhang [1998]. A major difficulty of this approach lies in the effort required to compute the statistical velocity

moments. A log conductivity field discretized by  $n_Y$  values requires the numerical solution of a multiple of  $n_Y$  moment-generating equations. Nonstationary (cross)-covariance matrices relating the fluctuations of discretized log conductivities, hydraulic heads and specific-discharge components need to be stored. Each of these matrices is sized  $n_Y \times n_Y$ . The numerical method of moments and its application to computing solute-flux statistical moments is thus restricted to fairly coarsely discretized domains. Three-dimensional applications, requiring many more cells or elements than two-dimensional ones, are difficult to handle.

[5] In the present study, we follow an alternative numerical approach in which we avoid the evaluation and storage of huge intermediate covariance matrices. We apply strict first-order propagation of uncertainty from discretized log conductivity values to simulated travel time values at observation points. We determine the sensitivity of the travel times with respect to the discretized log conductivity field by the adjoint-state method [Townley and Wilson, 1985; Sun and Yeh, 1990; Cirpka and Kitanidis, 2000a; James et al., 2000]. The sensitivities are the total derivatives of travel time with respect to the log conductivity values in all cells. Subsequently, we evaluate the covariance matrix of travel times at the observation points by quadratic multiplication of the log conductivity covariance matrix with the sensitivity matrix of travel times. Thus we apply a matrix-based first-order second-moment (FOSM) approach [Dettinger and Wilson, 1981].

[6] Applying FOSM to travel times has already been done by LaVenue et al. [1989], who, however, considered only a few discrete values of hydraulic conductivities corresponding to definite layers rather than many log conductivity values corresponding to a discretized auto-correlated field. Obviously, applying FOSM to large discretized domains, with  $n_Y$  ranging between  $10^5$  to  $10^6$ , one needs efficient methods for matrix calculations. For covariance matrices corresponding to stationary fields discretized on a regular grid, periodic embedding and multiplication in the Fourier domain has been shown to be very efficient [Nowak et al., 2003]. This technique can be applied directly to the evaluation of the travel time variance in fields where the nonstationarity of flow is not caused by the covariance of log conductivities. In the present study, we extend these methods to cases with nonstationary covariance functions of the log conductivity field that can be traced back to stationary counterparts. All matrix-multiplications are superfast ( $\mathcal{O}(n_p \log_2(n_p))$ ) in which  $n_p$  is the number of elements in the periodic domain, and not a single nonstationary covariance matrix of size  $n_Y \times n_Y$  needs to be stored.

## 2. Problem Statement

### 2.1. Governing Equations

[7] We consider steady state groundwater flow without internal volumetric sources or sinks, meeting the groundwater flow equation:

$$\nabla \cdot (K \nabla \phi) = 0 \quad (1)$$

in which  $K$  is the hydraulic conductivity, here assumed isotropic at the local scale, and  $\phi$  is the hydraulic head. The boundary  $\Gamma$  of the domain is subdivided into a section  $\Gamma_1$

with prescribed head values  $\hat{\phi}$ , and a remaining section  $\Gamma \setminus \Gamma_1$  with prescribed normal flux  $q_\Gamma$ :

$$\begin{aligned} \phi &= \hat{\phi} \text{ on } \Gamma_1 \\ -\mathbf{n} \cdot (K \nabla \phi) &= q_\Gamma \text{ on } \Gamma \setminus \Gamma_1 \end{aligned} \quad (2)$$

in which  $\mathbf{n}$  is a unit vector normal to the boundary pointing outward. The specific discharge vector throughout the domain is defined by Darcy's law:

$$\mathbf{q} = -K \nabla \phi \quad (3)$$

We consider advective-dispersive transport of an ideal tracer, not undergoing mass transfer or other reactive processes:

$$\theta \frac{\partial c}{\partial t} + \mathbf{q} \cdot \nabla c - \theta \nabla \cdot (\mathbf{D} \nabla c) = 0 \quad (4)$$

in which  $\theta$  is the (flow-effective) volumetric water content,  $c$  denotes concentration, and  $\mathbf{D}$  is the pore-scale dispersion tensor. For transport, the boundary is subdivided into the inflow boundary  $\Gamma_{in}$ , at which  $\mathbf{n} \cdot \mathbf{q}$  is negative, and the remaining section of the boundary  $\Gamma \setminus \Gamma_{in}$ . At inflow sections, we define an inflow flux concentration  $c_{in}$  as the boundary condition, whereas the dispersive flux is zero at all other boundary sections:

$$\begin{aligned} \mathbf{n} \cdot (\mathbf{q} c - \theta \mathbf{D} \nabla c) &= \mathbf{n} \cdot \mathbf{q} c_{in} & \text{on } \Gamma_{in} \\ \mathbf{n} \cdot (\mathbf{D} \nabla c) &= 0 & \text{on } \Gamma \setminus \Gamma_{in} \end{aligned} \quad (5)$$

[8] We characterize transport at a given observation point by the mean time a particle takes to travel from the inflow boundary to that point. This quantity has been used frequently in the Lagrangian analysis of solute-flux statistics [Shapiro and Cvetkovic, 1988; Dagan et al., 1992; Cvetkovic et al., 1992; Zhang et al., 2000]. Like Harvey and Gorelick [1995], we obtain the same quantity in an Eulerian context.

[9] In order to calculate the mean travel time of a particle arriving at an observation point, we imagine an experiment in which the tracer is introduced homogeneously into the flux over the entire inflow boundary, i.e.,  $c_{in} = \delta(t)m/Q$ . Here  $m$  is the total tracer mass and  $Q$  is the total discharge. Since the inflow concentration is considered uniform with respect to the lateral coordinate along the inflow boundary, the zeroth temporal moment of the concentration is uniform throughout the domain. The mean arrival time  $\tau(\mathbf{x})$  at any point  $\mathbf{x}$  within the domain is the first temporal moment normalized by the zeroth moment. For the given boundary conditions,  $\tau(\mathbf{x})$  meets the following steady state transport equation (see Appendix A):

$$\frac{\mathbf{q}}{\theta} \cdot \nabla \tau - \nabla \cdot (\mathbf{D} \nabla \tau) = 1 \quad (6)$$

$$\begin{aligned} \mathbf{n} \cdot (\mathbf{q} \tau - \theta \mathbf{D} \nabla \tau) &= 0 & \text{on } \Gamma_{in} \\ \mathbf{n} \cdot (\mathbf{D} \nabla \tau) &= 0 & \text{on } \Gamma \setminus \Gamma_{in} \end{aligned} \quad (7)$$

[10] Equation (6) gives the travel time to a point within the domain, regardless of the injection point. In the case of a

nonuniform injection of the tracer into the inflow, we would solve for the nonuniform distributions of the zeroth and first temporal moments. The travel time would subsequently be evaluated by normalizing the first moment with the zeroth. Extensions to steady state flow with source/sink terms and to transport with sorption are straightforward.

## 2.2. First-Order Second-Moment Approximation of Travel Time

[11] We consider the log conductivity  $Y = \ln(K)$  a random space variable characterized by second-order statistics:

$$\exp(\langle Y(\mathbf{x}_I) \rangle) = K_g(\mathbf{x}_I) \quad (8)$$

$$\langle Y'(\mathbf{x}_I)Y'(\mathbf{x}_{II}) \rangle = Q_{YY}(\mathbf{x}_I, \mathbf{x}_{II}) \quad (9)$$

in which  $\langle \cdot \rangle$  denotes the expected value of the argument, primed quantities denote deviations from the expected value,  $K_g(\mathbf{x}_I)$  is the geometric mean of the conductivity which may depend on the actual location  $\mathbf{x}_I$ , and  $Q_{YY}(\mathbf{x}_I, \mathbf{x}_{II})$  is the covariance function of the log conductivity fluctuations at locations  $\mathbf{x}_I$  and  $\mathbf{x}_{II}$ . In stationary media,  $K_g$  is uniform throughout the domain, and  $Q_{YY}$  depends only on the distance vector  $\mathbf{x}_{II} - \mathbf{x}_I$ .

[12] Since the travel time field  $\tau(\mathbf{x})$  depends on  $Y(\mathbf{x}_I)$ , it is also a random space variable which may be characterized by its expected value and covariance function. We get the zeroth-order approximation of  $\tau(\mathbf{x})$  in random heterogeneous media by calculating flow and transport with the field of the expected log conductivity values, keeping all other parameters, namely the dispersion coefficients, to their pore-scale values:

$$\tau^{(0)}(\mathbf{x}) = \tau(\mathbf{x}, K_g(\mathbf{x}_I)) \quad (10)$$

The zeroth-order approximation also holds as the first-order approximation of the mean, since the first-order terms are proportional to the log conductivity fluctuations  $Y'(\mathbf{x}_I)$  and cancel out when taking expected values. Second-order corrections of the mean require second derivatives of  $\tau(\mathbf{x})$  with respect to all log conductivity values  $Y'(\mathbf{x}_I)$ . Due to the accompanying high computational costs, these terms are not evaluated in the present study.

[13] The uncertainty in  $\tau(\mathbf{x})$  is given by simple error propagation [Dettinger and Wilson, 1981]:

$$Q_{\tau\tau}(\mathbf{x}, \mathbf{x}') = \int_{\Omega} \int_{\Omega} \frac{d\tau(\mathbf{x})}{dY(\mathbf{x}_I)} Q_{YY}(\mathbf{x}_I, \mathbf{x}_{II}) \frac{d\tau(\mathbf{x}')}{dY(\mathbf{x}_{II})} d\mathbf{x}_{II} d\mathbf{x}_I \quad (11)$$

in which  $Q_{\tau\tau}(\mathbf{x}, \mathbf{x}')$  is the covariance function of the travel time at locations  $\mathbf{x}$  and  $\mathbf{x}'$ , and  $d\tau(\mathbf{x})/dY(\mathbf{x}_I)$  is the sensitivity of  $\tau(\mathbf{x})$  with respect to  $Y(\mathbf{x}_I)$ , whereas  $\int_{\Omega} d\mathbf{x}$  denotes integration over the entire domain. When we discretize the log conductivity field in cells of constant values, we replace the double integral by a quadratic matrix-matrix multiplication:

$$\mathbf{Q}_{\tau\tau} = \mathbf{H}_{\tau} \mathbf{Q}_{YY} \mathbf{H}_{\tau}^T \quad (12)$$

in which  $\mathbf{Q}_{\tau\tau}$  is the covariance matrix of all considered  $\tau$  values and  $\mathbf{Q}_{YY}$  is the covariance matrix of the discretized

log conductivity values, whereas  $\mathbf{H}_{\tau}$  is the sensitivity matrix:

$$\mathbf{H}_{\tau} = \frac{d\tau}{d\mathbf{Y}^T} \quad (13)$$

with dimensions  $n_{\tau} \times n_Y$ . Here  $n_{\tau}$  is the number of travel time observations and  $n_Y$  denotes the number of log conductivity values.

## 2.3. Computational Effort

[14] Evaluating equation (12) by standard techniques is computationally demanding. Consider a typical two-dimensional domain discretized by  $\approx 10^4$  nodes. We may be interested in travel times at  $\approx 10^2$  outflow nodes. Then,  $\mathbf{Q}_{YY}$  has dimensions  $10^4 \times 10^4$ , whereas  $\mathbf{H}_{\tau}$  is a  $10^2 \times 10^4$  matrix. Using direct numerical differentiation, we would have to solve  $10^4$  flow- and transport-problems to evaluate the sensitivity matrix. These costs can be reduced to solving  $\mathcal{O}(10^2)$  flow and transport problems using adjoint-state methods [Townley and Wilson, 1985; Sun and Yeh, 1990; Cirpka and Kitanidis, 2000a; James et al., 2000]. The adjoint-state equations for the problem at hand are reviewed in section 3.

[15] With a nonstationary covariance matrix  $\mathbf{Q}_{YY}$ , it appears that we need to store all  $10^8$  entries (or at least, due to symmetry, one half of them). Using standard techniques, the matrix-matrix product in equation (12) would take  $\mathcal{O}[10^{10}]$  floating-point operations. This effort is prohibitive with respect to both storage and CPU time.

[16] For stationary media, it has been shown that the matrix multiplications mentioned above can be accelerated dramatically by periodic embedding of the covariance matrix [Golub and Loan, 1996; Nowak et al., 2003]. Each stationary covariance matrix, representing the correlation among values within a finite domain, can be interpreted as a submatrix of the covariance matrix belonging to a larger, periodic domain. For the latter, we can perform matrix-vector multiplications using Fast Fourier Transformation (FFT) techniques requiring only  $\mathcal{O}(n_p \log_2(n_p))$  floating-point operations, in which  $n_p$  is the number of nodes in the embedding periodic domain. In section 5, we briefly review these techniques. In section 6, we extend them to cases with certain types of nonstationary covariance matrices that we introduce in section 4.

## 3. Evaluation of Sensitivity Matrices

[17] In this section, we recall the calculation of sensitivity matrices by the continuous adjoint-state method [Sun and Yeh, 1990]. The steps in the derivation of the adjoint-state equations for the travel time  $\tau$  are listed in Appendix B. A more detailed description is given by Cirpka and Kitanidis [2000a] [see also James et al., 2000]. Here we only present the basic results. The general procedure is first to solve for the zeroth-order approximation of the flow and transport problem and then to evaluate adjoint-state equations. The sensitivities are finally computed by element-wise post-processing in a finite element context.

[18] For each type of measurement, we have to solve for one set of adjoint partial differential equations. The concentration moments depend, via the velocity field, on the log conductivity distribution. Since the velocity depends on

log conductivity both directly and indirectly via the hydraulic-head field, we need to solve for two adjoint states representing the two types of impact. The structures of the adjoint-state equations are very similar to the original equations: they consist of an adjoint transport equation and an adjoint flow equation.

[19] In the following, we denote the zeroth-order solution of the hydraulic head, specific discharge and travel time  $\phi^{(0)}$ ,  $\mathbf{q}^{(0)}$ , and  $\tau^{(0)}$  respectively. Consider a point-like observation of the arrival time at location  $\mathbf{x}_{0,\tau}$ . Then, the adjoint transport equation is:

$$-\frac{\mathbf{q}^{(0)}}{\theta} \cdot \nabla \psi_\tau - \nabla \cdot (\mathbf{D} \nabla \psi_\tau) = -\delta(\mathbf{x}_{0,\tau}) \quad (14)$$

subject to

$$\mathbf{n} \cdot (\mathbf{D} \nabla \psi_\tau) = 0 \text{ on } \Gamma \setminus \Gamma_{out} \quad (15)$$

$$\mathbf{n} \cdot \left( \psi_\tau \frac{\mathbf{q}^{(0)}}{\theta} + \mathbf{D} \nabla \psi_\tau \right) = 0 \text{ on } \Gamma_{out} \quad (16)$$

which is essentially identical to the forward transport equation of  $\tau^{(0)}$ , equation (6), with reversed direction of the flow field and a Dirac source term at the point of observation.  $\psi_\tau$  is the adjoint state of travel time, and  $\Gamma_{out}$  is the fraction of the boundary with an outward flow component in the forward problem, i.e.,  $\mathbf{q} \cdot \mathbf{n} > 0$ . The corresponding adjoint flow equation, representing the impact of log conductivity on the travel time via the hydraulic heads, is:

$$\nabla \cdot (K_g \nabla \psi_{\phi\tau}) = -\nabla \cdot \left( \nabla \tau^{(0)} \frac{K_g}{\theta} \psi_\tau \right) \quad (17)$$

subject to the boundary conditions:

$$\psi_{\phi\tau} = 0 \text{ on } \Gamma_1 \quad (18)$$

$$-\mathbf{n} \cdot (K_g \nabla \psi_{\phi\tau}) = \mathbf{n} \cdot \left( \nabla \tau^{(0)} \frac{K_g}{\theta} \psi_\tau \right) \text{ on } \Gamma \setminus \Gamma_1 \quad (19)$$

in which  $\psi_{\phi\tau}$  is an adjoint state of the hydraulic head in the context of travel time sensitivities. We consider element-wise constant values of log conductivity. Then, the sensitivity of the travel time  $\tau$  at location  $\mathbf{x}_{0,\tau}$  with respect to the log conductivity  $Y_\lambda$  in the element  $\lambda$  with volume  $V_\lambda$  is [Cirpka and Kitanidis, 2000a; James et al., 2000]:

$$\frac{\partial \tau(\mathbf{x}_{0,\tau})}{\partial Y_\lambda} = \int_{V_\lambda} \left[ -\frac{K_g}{\theta} \nabla \tau^{(0)} \cdot \nabla \phi^{(0)} \psi_\tau - K_g \nabla \psi_{\phi\tau} \cdot \nabla \phi^{(0)} \right] dV \quad (20)$$

We solve both the forward and the adjoint equations by the finite element method (FEM). In the simulation of flow, we apply the standard Galerkin technique for spatial discretization and solve the resulting system of linear equations by a conjugate-gradient method with algebraic multigrid preconditioning [Stüben, 2001]. We discretize the

temporal-moment generating equations by the Streamline-Upwind Petrov-Galerkin method [Brooks and Hughes, 1982], solving the resulting system of linear equations by the stabilized biconjugate gradient method with incomplete LU decomposition as preconditioner. All codes are written as Matlab scripts.

## 4. Covariance Matrices for Certain Cases of Nonstationarity

[20] In this section, we discuss covariance matrices of nonstationary media that can be traced back to stationary counterparts. We believe that most practical applications fall into this category. We discuss (1) nonstationarity due to variance scaling in which the variance has a spatial trend, (2) blending of two covariance matrices which includes the case of zonal stationarity, (3) nonstationarity because of uncertainty in trend parameters for the mean, and (4) nonstationarity due to conditioning.

### 4.1. Variance Scaling

[21] One of the simplest nonstationary models is based on variance scaling, in which the general shape of the covariance matrix is not altered but the variance is scaled by a trend function. This leads to the following expression:

$$\mathbf{Q}_{\mathbf{Y}\mathbf{Y}} = \mathbf{A} \mathbf{Q}_s \mathbf{A} \quad (21)$$

in which  $\mathbf{Q}_s$  is a  $n_Y \times n_Y$  symmetric positive-definite matrix representing the covariance matrix of a stationary, finite, discretized field.  $\mathbf{A}$  is a  $n_Y \times n_Y$  real diagonal scaling matrix. For the case of stationary media,  $\mathbf{A}$  is the identity matrix. A typical example of a nonstationary model is a linear trend of the variance with direction  $x_i$  requiring a square-root expression of  $x_i$  at the corresponding entry on the main diagonal of  $\mathbf{A}$ .

### 4.2. Blending of Two Covariance Matrices

[22] The covariance function of a random field may have a different shape in different parts of the domain. As an example, the integral scale may have a spatial trend. We can parameterize such situations by blending two (or more) covariance matrices:

$$\mathbf{Q}_{\mathbf{Y}\mathbf{Y}} = \mathbf{A}_1 \mathbf{Q}_1 \mathbf{A}_1 + \mathbf{A}_2 \mathbf{Q}_2 \mathbf{A}_2 \quad (22)$$

in which  $\mathbf{Q}_1$  and  $\mathbf{Q}_2$  are  $n_Y \times n_Y$  covariance matrices of stationary fields, whereas  $\mathbf{A}_1$  and  $\mathbf{A}_2$  are  $n_Y \times n_Y$  real diagonal matrices. The simplest blending model represents zonal stationarity, in which the diagonal entries of  $\mathbf{A}_1$  and  $\mathbf{A}_2$  are either zero or one, and the sum  $\mathbf{A}_1 + \mathbf{A}_2$  is the identity matrix.

### 4.3. Marginal Covariance Matrix for Uncertain Trend Parameters of the Mean

[23] Consider a trend model describing the expected value of the log conductivity field  $Y(\mathbf{x})$ :

$$E[\mathbf{Y}] = \mathbf{X} \boldsymbol{\beta} \quad (23)$$

in which  $\boldsymbol{\beta}$  is a  $n_b \times 1$  vector of trend parameters with the number of trend parameters  $n_b$ , and  $\mathbf{X}$  is a  $n_Y \times n_b$  matrix of discretized base functions with entries that depend

on the location  $\mathbf{x}$  at which the log conductivity  $Y(\mathbf{x})$  is considered. For known trend parameters  $\beta$ , we assume  $\mathbf{Y}$  to fluctuate about  $\mathbf{X}\beta$  with a multi-Gaussian distribution. The corresponding covariance function  $Q_{YY}(\mathbf{x}_I, \mathbf{x}_{II})$  is not necessarily stationary. In addition, the trend parameters  $\beta$  may be uncertain. To account for the uncertainty of  $\beta$ , we assume a multi-Gaussian distribution of  $\beta$  with prior mean  $\beta^*$  and covariance  $\mathbf{Q}_{\beta\beta}$ . Marginalization leads to the marginal mean  $\tilde{\mathbf{Y}}$  and the marginal covariance  $\mathbf{G}_{\mathbf{Y}\mathbf{Y}}$  of  $\mathbf{Y}$  with uncertain value of the drift coefficients  $\beta$ :

$$\tilde{\mathbf{Y}} = \mathbf{X}\beta^* \quad (24)$$

$$\mathbf{G}_{\mathbf{Y}\mathbf{Y}} = \mathbf{Q}_{\mathbf{Y}\mathbf{Y}} + \mathbf{X}\mathbf{Q}_{\beta\beta}\mathbf{X}^T \quad (25)$$

Equation (25) exemplifies the fact that the marginal covariance  $\mathbf{G}_{\mathbf{Y}\mathbf{Y}}$  of  $\mathbf{Y}$  without exact knowledge of  $\beta$  is larger than the covariance  $\mathbf{Q}_{\mathbf{Y}\mathbf{Y}}$  for known  $\beta$  values. Even if  $\mathbf{Q}_{\mathbf{Y}\mathbf{Y}}$  is stationary, the marginal  $\mathbf{G}_{\mathbf{Y}\mathbf{Y}}$  may be nonstationary because of the spatial dependence in the underlying trend model.

[24] If there is no information on the trend parameters whatsoever, i.e.,  $\mathbf{Q}_{\beta\beta}^{-1} = \mathbf{0}$ , the marginal variance of  $Y$  is infinite, and the marginal covariance matrix  $\mathbf{G}_{\mathbf{Y}\mathbf{Y}}$  is a generalized rather than a regular matrix. The inverse  $\mathbf{G}_{\mathbf{Y}\mathbf{Y}}^{-1}$ , however, is still regular [e.g., *Kitanidis*, 1995, and references therein]:

$$\mathbf{G}_{\mathbf{Y}\mathbf{Y}}^{-1} = \mathbf{Q}_{\mathbf{Y}\mathbf{Y}}^{-1} - \mathbf{Q}_{\mathbf{Y}\mathbf{Y}}^{-1}\mathbf{X}(\mathbf{X}^T\mathbf{Q}_{\mathbf{Y}\mathbf{Y}}^{-1}\mathbf{X})^{-1}\mathbf{X}^T\mathbf{Q}_{\mathbf{Y}\mathbf{Y}}^{-1} \quad (26)$$

#### 4.4. Conditional Covariance Matrix

[25] Conditioning a random space function by measurements of either the function itself or a dependent quantity is a classical case in which a potentially stationary field becomes nonstationary. As an example, we may consider measurements of the hydraulic head  $\phi$  that are used to condition the log conductivity field  $Y$ . In the following, we denote the  $m \times 1$  vector of the measured quantity at the  $m$  measurement points by  $\mathbf{Z}$ ; the measurements themselves, which may be prone to a measurement error, are denoted  $\mathbf{Z}^m$ . The covariance matrix of the measurement errors is denoted  $\mathbf{R}_{\mathbf{Z}\mathbf{Z}}$ . We evaluate the conditional mean, or best estimate,  $\hat{\mathbf{Y}}$  and the conditional, or posterior, covariance matrix  $\mathbf{Q}_{\mathbf{Y}\mathbf{Y}|\mathbf{Z}^m}$  of  $\mathbf{Y}$  given  $\mathbf{Z}^m$  by the quasi-linear method of geostatistical inverting as outlined by *Kitanidis* [1995]. The estimate  $\hat{\mathbf{Y}}$  is given in the function estimate form:

$$\hat{\mathbf{Y}}_{k+1} = \mathbf{X}\hat{\beta}_{k+1} + \mathbf{Q}_{\mathbf{Y}\mathbf{Y}}\mathbf{H}_{\mathbf{Z},k}^T\zeta_{k+1} \quad (27)$$

in which  $\hat{\beta}_{k+1}$  is the estimate of the trend parameters after the  $(k+1)$ -th iteration,  $\mathbf{H}_{\mathbf{Z},k}$  is the  $n_Y \times m$  sensitivity matrix of the measured quantity with respect to the  $Y$  field evaluated at the previous estimate  $\hat{\mathbf{Y}}_k$ , and  $\zeta_{k+1}$  is a  $m \times 1$  vector of weights associated with the measurements. The vectors  $\hat{\beta}_{k+1}$  and  $\zeta_{k+1}$  are determined by solving the cokriging system of equations:

$$\begin{bmatrix} \mathbf{H}_{\mathbf{Z},k}\mathbf{Q}_{\mathbf{Y}\mathbf{Y}}\mathbf{H}_{\mathbf{Z},k}^T + \mathbf{R}_{\mathbf{Z}\mathbf{Z}} & \mathbf{H}_{\mathbf{Z},k}\mathbf{X} \\ \mathbf{X}^T\mathbf{H}_{\mathbf{Z},k}^T & -\mathbf{Q}_{\beta\beta}^{-1} \end{bmatrix} \begin{bmatrix} \zeta_{k+1} \\ \hat{\beta}_{k+1} \end{bmatrix} = \begin{bmatrix} \mathbf{Z}^m - \mathbf{Z}(\hat{\mathbf{Y}}_k) + \mathbf{H}_{\mathbf{Z},k}\hat{\mathbf{Y}}_k \\ -\mathbf{Q}_{\beta\beta}^{-1}\beta^* \end{bmatrix} \quad (28)$$

in which  $\mathbf{Z}(\hat{\mathbf{Y}}_k)$  is the model prediction for the measured quantity, applying the previous estimate  $\hat{\mathbf{Y}}_k$ . The iterative cokriging procedure has to be repeated until convergence is reached. We stabilize the method further by adopting the Levenberg-Marquardt algorithm for underdetermined problems (W. Nowak and O. Cirpka, A modified Levenberg-Marquardt algorithm for application to iterative cokriging, submitted to *Advances in Water Resources*, 2003). It can be shown that the cokriging solution is the Bayesian update of the prior field  $\tilde{\mathbf{Y}}$  conditioned on the dependent data  $\mathbf{Z}^m$  [*Kitanidis*, 1995]. Equation (28) is written here for uncertain rather than completely unknown trend parameters. Should there be no prior information on the drift coefficients  $\beta$ , the corresponding inverse covariance matrix  $\mathbf{Q}_{\beta\beta}^{-1}$  is a zero matrix.

[26] A lower bound of the conditional covariance  $\mathbf{Q}_{\mathbf{Y}\mathbf{Y}|\mathbf{Z}^m}$  is given by:

$$\mathbf{Q}_{\mathbf{Y}\mathbf{Y}|\mathbf{Z}^m} \geq \mathbf{Q}_{\mathbf{Y}\mathbf{Y}} - \begin{bmatrix} \mathbf{H}_{\mathbf{Z}}\mathbf{Q}_{\mathbf{Y}\mathbf{Y}} \\ \mathbf{X}^T \end{bmatrix}^T \begin{bmatrix} \mathbf{H}_{\mathbf{Z}}\mathbf{Q}_{\mathbf{Y}\mathbf{Y}}\mathbf{H}_{\mathbf{Z}}^T + \mathbf{R}_{\mathbf{Z}\mathbf{Z}} & \mathbf{H}_{\mathbf{Z}}\mathbf{X} \\ \mathbf{X}^T\mathbf{H}_{\mathbf{Z}}^T & -\mathbf{Q}_{\beta\beta}^{-1} \end{bmatrix}^{-1} \begin{bmatrix} \mathbf{H}_{\mathbf{Z}}\mathbf{Q}_{\mathbf{Y}\mathbf{Y}} \\ \mathbf{X}^T \end{bmatrix} \quad (29)$$

which is exact for linear problems. It is quite obvious that the conditional covariance matrix is nonstationary even when the unconditional covariance  $\mathbf{Q}_{\mathbf{Y}\mathbf{Y}}$  is stationary. When  $\mathbf{Q}_{\mathbf{Y}\mathbf{Y}}$  is nonstationary, efficient matrix multiplications are not only needed for further error propagation of the conditional covariance matrix  $\mathbf{Q}_{\mathbf{Y}\mathbf{Y}|\mathbf{Z}^m}$  but also for the evaluation of  $\mathbf{H}_{\mathbf{Z}}\mathbf{Q}_{\mathbf{Y}\mathbf{Y}}$  and  $\mathbf{H}_{\mathbf{Z}}\mathbf{Q}_{\mathbf{Y}\mathbf{Y}}\mathbf{H}_{\mathbf{Z}}^T$  occurring in the cokriging equations, equations (27) and (28).

## 5. Periodic Embedding

### 5.1. Structure of the Covariance Matrices of Stationary and Periodic Fields

[27] In the discussion above, we have shown that several important cases of nonstationary covariance functions can be traced back to stationary counterparts, the latter being invariant to translation. Consider the spatial discretization on a regular grid as is quite common, for example when using a Finite Differences scheme. Then, the covariance matrix  $\mathbf{Q}_s$  of a stationary field includes only a limited set of values representing the covariance function for the repeated distance vectors between two points on the grid. The entire covariance matrix can be constructed from the covariance relating the cell in the lower left corner to all other cells. Mathematically, the covariance matrix of a regularly discretized stationary field has block-Toeplitz structure with Toeplitz blocks [*Dietrich and Newsam*, 1997].

[28] The structure of the matrix is extremely important. Consider a three-dimensional domain discretized by  $10^6$  nodes. Then, the full covariance matrix would have  $10^{12}$  entries which is beyond the storage capacity of any contemporary computer. If we consider the block-Toeplitz structure of the covariance matrix, we need to store only  $10^6$  entries.

[29] A mathematically even more convenient, structured matrix is circulant. A circulant covariance matrix describes the covariance among the entries of a discretized unit cell within a periodic domain. Here all values repeat themselves

at distances that are an integer multiple of the unit cell's length  $\ell$ . When the distance  $h$  approaches the unit cell's length  $\ell$ , the parameters become increasingly correlated. In fact, the following identity holds:

$$Q_c(\ell - h) = Q_c(h) \quad (30)$$

In multidimensional applications, periodicity is enforced in all directions, leading to block-circulant matrices with circulant blocks. As we will see in the following, it is computationally efficient to embed a nonperiodic finite domain with spatially invariant statistics (and a Toeplitz covariance matrix) in a virtual, larger, periodic field (with a circulant covariance matrix) [Dietrich and Newsam, 1997]. In practical applications, one generates the first line of the circulant covariance matrix directly from the periodic covariance function.

[30] Formally, we can write the construction of a stationary covariance from the periodic counter-part as:

$$\mathbf{Q}_s = \mathbf{M}^T \mathbf{Q}_p \mathbf{M} \quad (31)$$

in which the  $n_p \times n_Y$  mapping matrix  $\mathbf{M}$  transfers the entries of the finite stationary domain to those of the periodic domain.  $n_p$  is the number of entries in the embedding periodic domain.  $\mathbf{M}$  has a single entry of unity per column.  $\mathbf{M}^T$  extracts the entries occurring in the stationary field from those in the periodic field. In practice, a multiplication  $\mathbf{M}\mathbf{u}$  implies mapping the entries of the finite domain onto the unit cell of the periodic domain. All entries in the periodic domain that do not exist in the finite domain are filled in by zeros (zero padding). Likewise, the operation  $\mathbf{M}^T \mathbf{u}_p$  is carried out by extracting those entries of the periodic field  $\mathbf{u}_p$  that also occur in the finite field, discarding the extra entries.

## 5.2. Matrix-Vector and Matrix-Matrix Multiplications

[31] In the following, we will apply the discrete Fourier transformation as implemented in Matlab (<http://www.ffmpeg.org>). The Fourier transform of a periodic field  $\mathbf{u}_p$  is denoted  $\tilde{\mathbf{u}}_p = \mathcal{F}(\mathbf{u}_p)$ , and the inverse Fourier transformation  $\mathbf{u}_p = \mathcal{F}^{-1}(\tilde{\mathbf{u}}_p)$ . The diagonalization theorem states that the eigenvalues of a circulant matrix are identical to the Fourier transform of the first column of the matrix. As a consequence, a matrix-vector product involving a circulant matrix becomes [see Golub and Loan, 1996, p. 202]:

$$\mathbf{Q}_p \mathbf{u}_p = \mathcal{F}^{-1}(\mathcal{F}(\mathbf{q}_1) \circ \mathcal{F}(\mathbf{u}_p)) \quad (32)$$

in which  $\mathbf{a} \circ \mathbf{b}$  is the Hadamard product, i.e., the element-wise multiplication of vectors  $\mathbf{a}$  and  $\mathbf{b}$ , whereas  $\mathbf{q}_1$  is the first column of  $\mathbf{Q}_p$ .

[32] Formally, we may write the multiplication of a Toeplitz matrix with a vector as:

$$\begin{aligned} \mathbf{Q}_s \mathbf{u} &= \mathbf{M}^T \mathbf{Q}_p \mathbf{M} \mathbf{u} \\ &= \mathbf{M}^T \mathcal{F}^{-1}(\mathcal{F}(\mathbf{q}_1) \circ \mathcal{F}(\mathbf{M}\mathbf{u})) \end{aligned} \quad (33)$$

which implies that we have to embed the vector  $\mathbf{u}$ , here representing entries on a discretized finite domain with

stationary covariance function, in a larger vector  $\mathbf{u}_p = \mathbf{M}\mathbf{u}$  in the corresponding periodic domain. The new entries are padded with zeros. Now we apply the circulant matrix-vector product, equation (32), i.e., we take the discrete, multidimensional Fourier transform of  $\mathbf{u}_p$  and multiply each entry with the Fourier transform of  $\mathbf{q}_1$ . After back-transformation into the spatial domain, we extract the part of the resulting expression that is related to the finite stationary field [Dietrich and Newsam, 1997; Nowak et al., 2003]. The multiplication thus requires three fast Fourier transformations (FFT), each with a computational effort of  $\mathcal{O}(n_p \log_2(n_p))$ , whereas the traditional matrix-vector product requires  $\mathcal{O}(n_p^2)$  operations. Hence the periodic embedding is advantageous for large domains, even when the periodic domain has four times the number of entries occurring in the finite stationary domain.

[33] In matrix-matrix multiplications, we consider each column of the right-hand matrix separately. With  $m$  columns, we need  $(2m + 1)$  FFT operations. Consider the quadratic matrix-matrix product in equation (12),  $\mathbf{Q}_{\tau\tau} = \mathbf{H}_\tau \mathbf{Q}_{YY} \mathbf{H}_\tau^T$ , for a covariance matrix  $\mathbf{Q}_{YY}$  corresponding to a stationary covariance function of the log conductivity field. A nonuniform mean in the log conductivity or boundary conditions in the flow problem may lead to a nonstationary velocity field. In that case,  $d\tau(\mathbf{x}_I)/dY(\mathbf{x}_{II})$  depends on the actual position of  $\mathbf{x}_I$  and  $\mathbf{x}_{II}$  rather than on the separation vector  $\mathbf{x}_{II} - \mathbf{x}_I$ . This means that the sensitivity matrix  $\mathbf{H}_\tau$  does not exhibit a simple structure, whereas the covariance matrix of the log conductivity values  $\mathbf{Q}_{YY}$  is a Toeplitz matrix. The calculation of the covariance matrix  $\mathbf{Q}_{\tau\tau}$  of travel time observations  $\tau$  may be written formally by substituting equation (31) in equation (12):

$$\mathbf{Q}_{\tau\tau} = \mathbf{H}_\tau \mathbf{M}^T \mathbf{Q}_p \mathbf{M} \mathbf{H}_\tau^T \quad (34)$$

Using Fourier-transformation techniques, equation (33), the terms of  $\mathbf{Q}_{\tau\tau}$  are evaluated by:

$$Q_{\tau_i\tau_j} = \mathbf{h}_{\tau_i} \mathbf{M}^T \mathcal{F}^{-1}(\mathcal{F}(\mathbf{q}_1) \circ \mathcal{F}(\mathbf{M}\mathbf{h}_{\tau_j}^T)) \quad (35)$$

in which  $\mathbf{h}_{\tau_i}$  is the  $i$ -th row of the sensitivity matrix  $\mathbf{H}_\tau$ . In the physical context,  $\mathbf{h}_{\tau_i}$  is the sensitivity of the  $i$ -th travel time observation with respect to all log conductivity values in the finite stationary domain. We perform the multiplication  $\mathbf{Q}_{YY} \mathbf{h}_{\tau_j}^T$  for each sensitivity field  $\mathbf{h}_{\tau_j}$  by applying equation (32), and subsequently multiply the resulting matrix by the full sensitivity matrix  $\mathbf{H}_\tau$ . The principles of this procedure have already been described earlier [Golub and Loan, 1996; Nowak et al., 2003].

[34] It may be worth noting that the principles of periodic embedding can also be used for fields that are characterized by a power law variogram [Zhang, 2002, pp. 76–81]. In this case, we extend the variogram for distances larger than the domain size such that it asymptotically approaches a finite variance, here denoted  $\delta^2$ . We transform the extended variogram to a regular covariance function  $\tilde{Q}_{YY}(\mathbf{x}_I - \mathbf{x}_{II})$ , which can be embedded in a periodic domain. The discrete cross-variogram matrix

$\Gamma_{Y\tau} = \Gamma_{YY}\mathbf{H}_\tau^T$  of the discretized log conductivity values  $\mathbf{Y}$  and the travel time observations  $\tau$  is then given by:

$$\Gamma_{Y\tau} = \Gamma_{YY}\mathbf{H}_\tau^T = \check{\sigma}^2\mathbf{U}\mathbf{H}_\tau^T - \check{\mathbf{Q}}_{YY}\mathbf{H}_\tau^T \quad (36)$$

in which  $\Gamma_{YY}$  is the variogram matrix of the discretized log conductivity values, and  $\mathbf{U}$  is a matrix containing unit entries only.  $\check{\mathbf{Q}}_{YY}$  is the discrete form of  $\check{Q}_{YY}(\mathbf{x}_I - \mathbf{x}_{II})$  for all points within the domain, and the matrix-matrix product  $\check{\mathbf{Q}}_{YY}\mathbf{H}_\tau^T$  is computed by applying equation (32) to each row of  $\mathbf{H}_\tau$ .

## 6. Evaluation of First-Order Second Moments Involving Matrices of Discretized Nonstationary Covariance Functions

[35] In this section, we discuss the evaluation of the first-order travel time variance for the cases of nonstationarity in the log conductivity field discussed in section 4. We first analyze the case in which nonstationarity in the covariance function appears due to variance scaling, as described in section 4.1. Substituting equation (21) in equations (31) and (12) yields:

$$\mathbf{Q}_{\tau\tau} = \mathbf{H}_\tau\mathbf{A}\mathbf{M}^T\mathbf{Q}_p\mathbf{M}\mathbf{A}\mathbf{H}_\tau^T \quad (37)$$

which can be traced back to the stationary case under application of an auxiliary matrix  $\mathbf{L}$ :

$$\mathbf{L} = \mathbf{H}_\tau\mathbf{A} \quad (38)$$

leading to:

$$\mathbf{Q}_{\tau\tau} = \mathbf{L}\mathbf{M}^T\mathbf{Q}_p\mathbf{M}\mathbf{L}^T \quad (39)$$

[36] This is identical to the stationary case, using  $\mathbf{L}$  rather than  $\mathbf{H}_\tau$ . Obviously, it is advantageous to perform the multiplication  $\mathbf{L} = \mathbf{H}_\tau\mathbf{A}^T$  prior to the quadratic multiplication with the stationary covariance matrix  $\mathbf{M}^T\mathbf{Q}_p\mathbf{M}$ . Since  $\mathbf{A}$  is a diagonal matrix, we need to store only  $n_Y$  entries, and the evaluation of the auxiliary matrix  $\mathbf{L}$  can be done by element-wise multiplication of the sensitivity matrix  $\mathbf{H}_\tau$  with the spatial scaling factor included in  $\mathbf{A}$ . The remaining multiplication of  $\mathbf{M}^T\mathbf{Q}_p\mathbf{M}$  and  $\mathbf{L}^T$  is performed by the same Fourier-transformation technique as applied in equation (35):

$$Q_{\tau_i\tau_j} = \ell_i\mathbf{M}^T\mathcal{F}^{-1}\left(\mathcal{F}(\mathbf{q}_1) \circ \mathcal{F}(\mathbf{M}\ell_j^T)\right) \quad (40)$$

in which  $\ell_i$  is the  $i$ th row of matrix  $\mathbf{L}$ .

[37] When we blend two covariance matrices, as explained in section 4.2, we perform the variance scaling with two or more stationary covariance matrices and sum up the resulting terms, see equation (22). Consequently, we can perform the uncertainty propagation from log conductivity to travel time values for each stationary submatrix as outlined above and sum up the matrices.

[38] Next, we consider nonstationarity due to marginalization, using a nonuniform trend model as described in section 4.3. If the vector of drift coefficients  $\beta$  is uncertain,

the uncertainty in  $\tau$  increases accordingly. Substituting equation (25) in equation (12) yields:

$$\mathbf{Q}_{\tau\tau} = \mathbf{H}_\tau\mathbf{G}_{YY}\mathbf{H}_\tau^T = \mathbf{H}_\tau\mathbf{Q}_{YY}\mathbf{H}_\tau^T + \underbrace{\mathbf{H}_\tau\mathbf{X}}_{=\mathbf{L}}\mathbf{Q}_{\beta\beta}\underbrace{\mathbf{X}^T\mathbf{H}_\tau^T}_{=\mathbf{L}^T} \quad (41)$$

The first term,  $\mathbf{H}_\tau\mathbf{Q}_{YY}\mathbf{H}_\tau^T$ , has been discussed above. For the second term, it is advantageous to perform the calculation  $\mathbf{H}_\tau\mathbf{X}$  prior to the quadratic multiplication with  $\mathbf{Q}_{\beta\beta}$ , since  $\mathbf{Q}_{\beta\beta}$  is sized  $n_b \times n_b$  and  $\mathbf{H}_\tau\mathbf{X}$  is sized  $n_\tau \times n_b$ . There is no need to evaluate the huge  $n_Y \times n_Y$  matrix  $\mathbf{X}\mathbf{Q}_{\beta\beta}\mathbf{X}^T$ . If  $\beta$  is completely unknown,  $\mathbf{Q}_{\beta\beta}$  has entries of infinite value, and the uncertainty in travel times is also infinite.

[39] Finally, we may consider nonstationarity in the log conductivity field due to conditioning, as described in section 4.4. Substituting equation (29) into equation (12) yields:

$$\begin{aligned} \mathbf{Q}_{\tau\tau|Z^m} &= \mathbf{H}_\tau\mathbf{Q}_{YY|Z^m}\mathbf{H}_\tau^T \\ &= \mathbf{H}_\tau\mathbf{Q}_{YY}\mathbf{H}_\tau^T - \mathbf{L}\left[\begin{array}{cc} \mathbf{H}_Z\mathbf{Q}_{YY}\mathbf{H}_Z^T + \mathbf{R}_{ZZ} & \mathbf{H}_Z\mathbf{X} \\ \mathbf{X}^T\mathbf{H}_Z^T & -\mathbf{Q}_{\beta\beta} \end{array}\right]^{-1}\mathbf{L}^T \end{aligned} \quad (42)$$

$$\text{with } \mathbf{L} = \mathbf{H}_\tau\left[\begin{array}{c} \mathbf{H}_Z\mathbf{Q}_{YY} \\ \mathbf{X}^T \end{array}\right]^T$$

in which  $\mathbf{Q}_{\tau\tau|Z^m}$  is the conditional covariance matrix of the travel time at the observation points, given the measurements  $Z^m$ . It may be worth noting that the sensitivity matrix  $\mathbf{H}_\tau$  differs in the unconditional and the conditional cases. The term  $\mathbf{H}_\tau\mathbf{Q}_{YY}\mathbf{H}_\tau^T$  can be evaluated by the methods discussed above. For the remaining contribution to  $\mathbf{Q}_{\tau\tau|Z^m}$ , there is no need to store the complete conditional covariance  $\mathbf{Q}_{YY|Z^m}$  of the log conductivity values, given the measurements  $Z^m$ . Instead, one should perform the calculation of the  $n_\tau \times (m + n_p)$  auxiliary matrix  $\mathbf{L} = \mathbf{H}_\tau[\mathbf{Q}_{YY}\mathbf{H}_Z^T, \mathbf{X}]$  first, and subsequently perform the quadratic multiplication with the inverse of the  $(m + n_b) \times (m + n_b)$  cokriging matrix. The matrix products  $\mathbf{H}_Z\mathbf{Q}_{YY}$  and  $\mathbf{H}_Z\mathbf{Q}_{YY}\mathbf{H}_Z^T$  appearing in the cokriging equations may be computed with the same embedding and Fourier-transformation techniques discussed in this paper for  $\mathbf{H}_\tau\mathbf{Q}_{YY}\mathbf{H}_\tau^T$ .

## 7. Illustrative Examples

[40] We demonstrate the performance of our method with two example applications. Both of them describe a two-dimensional aquifer of size 100 m  $\times$  50 m discretized by 1000  $\times$  500 elements with piecewise constant log conductivity values. Mean flow is from the left to the right. The mean hydraulic gradient is one per cent. The line of travel time observations is located at  $x_1 = 90$  m. We consider 50 equally distributed observation points.

### 7.1. Travel Time Variance for a Formation With Zonal Stationarity

[41] In the first application, we consider a domain made of two materials with differing mean values and covariance functions of the conductivity. Within both materials, the log conductivity is stationary. Figure 1a shows the known distribution of the materials. The white areas are occupied

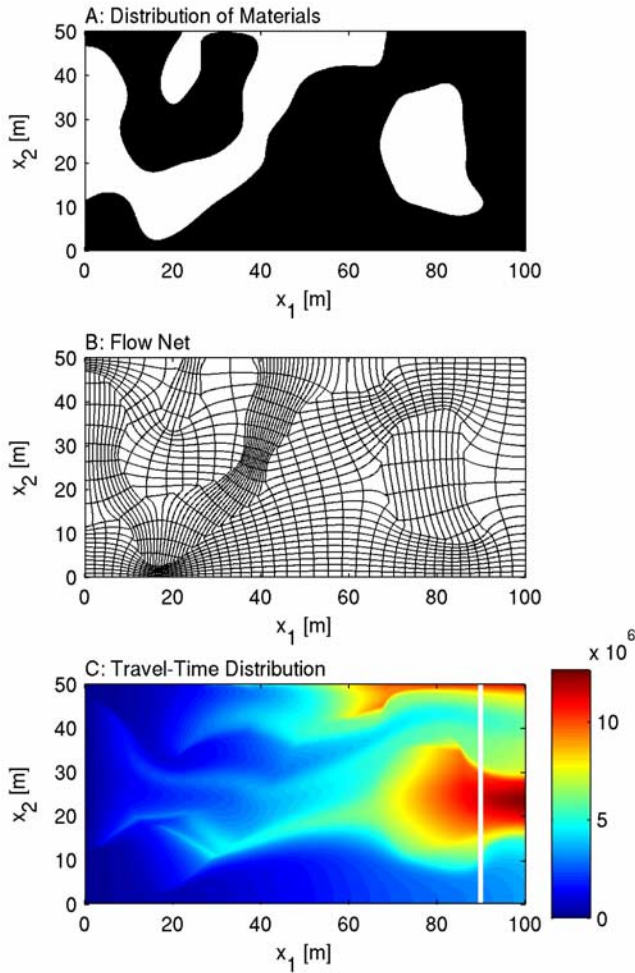


**Figure 1.** Application 1: (a) Distribution of materials, (b) flow net, and (c) expected value of travel time distribution. White line in Figure 1c is the control plane for travel time observations.

by material 1 with a geometric mean of the conductivity of  $10^{-4}$  m/s. In the black areas, we find material 2 with a higher mean conductivity of  $10^{-3}$  m/s. The materials also differ in their variance and spatial correlation, material 1 being less variable and exhibiting spatial correlation with a smaller integral scale than material 2. For both materials, we have assumed an isotropic exponential covariance function. All relevant parameters are listed in Table 1.

[42] Figure 1b shows the mean flow net in the aquifer, for fixed-head conditions to the left and right boundaries and no-flow conditions to the top and bottom boundaries. It is evident that the mean flow passes around the low-conductivity zones. The velocities in these zones are significantly lower than in the high-conductivity regions. The complex flow pattern results in the distribution of mean travel times shown in Figure 1c. In the low-conductivity zones, the travel time increases dramatically over small travel distances but remains small in the high-conductivity areas. Where the two materials form an interface parallel to the direction of flow, we observe strong transverse gradients of travel time which are smoothed out only by transverse dispersion.

**Table 1.** Parameters for Application 1: Zonal Stationarity

Parameter	Value
<i>Geometry of the Domain</i>	
Domain size	$L_1 = 100$ m, $L_2 = 50$ m
Discretization	$\Delta x_1 = 0.1$ m, $\Delta x_2 = 0.1$ m
<i>Geostatistical Parameters of Log Conductivity in the Zones<sup>a</sup></i>	
<b>Zone 1</b>	
Mean log conductivity	$E[Y_1] = \ln(10^{-4})$
Type of covariance model	isotropic exponential
Variance	$\sigma_Y^2 = 0.5$
Correlation length	$\lambda = 2$ m
<b>Zone 2</b>	
Mean log conductivity	$E[Y_2] = \ln(10^{-3})$
Type of covariance model	isotropic exponential
Variance	$\sigma_Y^2 = 1.0$
Correlation length	$\lambda = 10$ m
<i>Boundary Conditions for Flow</i>	
Top boundary	no flow
Bottom boundary	no flow
Left boundary	$\phi = 1$ m
Right boundary	$\phi = 0$ m
<i>Transport Parameters</i>	
Porosity	$\theta = 0.3$
Eff. diffusion coefficient	$D_e = 10^{-9}$ m <sup>2</sup> /s
Longitudinal dispersivity	$\alpha_L = 0.01$ m
Transverse dispersivity	$\alpha_T = 0.01$ m
<i>Locations of Travel Time Observation</i>	
Longitudinal coordinate	$x_1 = 90$ m
Transverse coordinates	$y_2 = 1$ m, 3 m, 5 m, ..., 49 m

<sup>a</sup>Distribution of materials is according to pattern shown in Figure 1.

[43] Figure 2 shows the profile of the mean travel time  $\tau^{(0)}$ , which is subject to the known distribution of the two materials shown in Figure 1a, and the corresponding standard deviation  $\sigma_\tau$  along the line of observation at  $x_1 = 90$  m. The standard deviation is evaluated by the FOSM approach outlined in the previous sections. In agreement with Figure 1c we see a strong gradient of travel time at

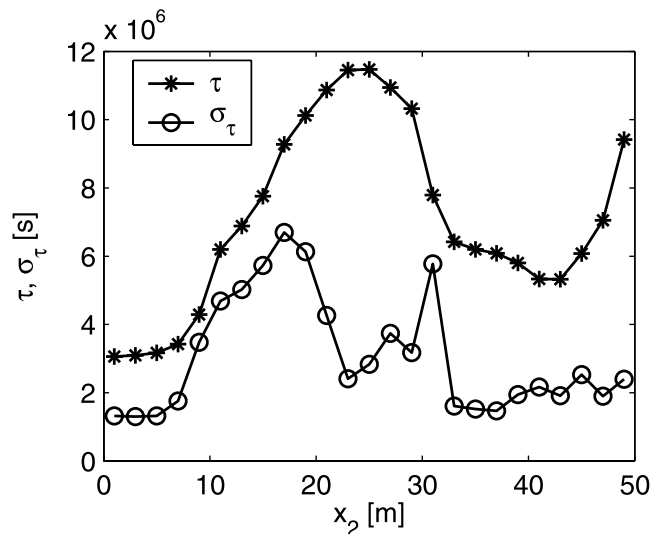


**Figure 2.** Application 1: Profile of travel time on the control plane. Asterisks are expected value; circles are standard deviation.

$x_2 \approx 30$  m. Here we observe a local maximum of the first-order standard deviation  $\sigma_\tau$ . Intuitively, this local maximum makes sense. Although small fluctuations in the log conductivity field will cause only small fluctuations of the streamline pattern, the latter may cause significant fluctuations in the travel time when the mean travel time shows a strong transverse gradient.

[44] The overall profile of  $\sigma_\tau$ , however, is nontrivial. From the Lagrangian analysis of travel time variance [Zhang *et al.*, 2000], it is clear that  $\sigma_\tau^2$  is essentially a cumulative measure of the velocity uncertainty sampled along the trajectory leading to the observation point. Thus the differences in the profile of  $\sigma_\tau$  reflect cumulated differences in the velocity covariance upstream of the observation plane, and the  $\sigma_\tau$ -profile cannot be explained by local effects on the observation plane alone.

## 7.2. Unconditional and Conditional Travel Time Variance for a Formation With Continuous Blending of Two Covariance Functions

[45] In the second application, we consider a domain similar to in the first one. In this case, however, we assume a covariance function that is generated by continuous blending of two stationary functions. These functions are both of the Gaussian type, reflecting small-scale structures with low variability in function 1 and large-scale structures with high variability in function 2. The blending leads to a linear transition of the variance in the transverse direction:

$$Q_{YY}(\mathbf{x}_I, \mathbf{x}_{II}) = \sqrt{\left(1 - \frac{x_{I,2}}{L_2}\right) \left(1 - \frac{x_{II,2}}{L_2}\right) \sigma_1^2 \exp\left(-\frac{(\mathbf{x}_I - \mathbf{x}_{II}) \cdot (\mathbf{x}_I - \mathbf{x}_{II})}{\lambda_1^2}\right)} + \sqrt{\frac{x_{I,2}}{L_2} \frac{x_{II,2}}{L_2} \sigma_2^2 \exp\left(-\frac{(\mathbf{x}_I - \mathbf{x}_{II}) \cdot (\mathbf{x}_I - \mathbf{x}_{II})}{\lambda_2^2}\right)} \quad (43)$$

[46] In this application, we will cover several aspects. First, we show the effect of nonstationarity in the covariance function under otherwise uniform conditions, i.e., uniform mean log conductivity and hydraulic gradient. Second, we show that uncertainty in the mean log conductivity leads to a dramatic increase in the uncertainty of travel time. Third, we condition the log conductivity field on accurate measurements of hydraulic head and fairly inaccurate measurements of the log conductivity itself. We show how these measurements reduce the uncertainty of travel time predictions in a nonstationary manner. All relevant parameters are listed in Table 2.

[47] Figure 3 shows the log conductivity distributions, the flow nets, and the travel time distributions for a single realization, the prior mean, and the conditional mean after zhead and log conductivity measurements have been accounted for. The related travel time profiles along the observation plane are plotted in Figure 4. The corresponding variances are shown in Figure 5.

[48] The log conductivity field of the particular realization shown in Figure 3, plot A1, illustrates the effect of covariance blending. The structures at the top of the domain are significantly larger than those at the bottom. The resulting flow net, shown in Figure 3, plot A2, and

**Table 2.** Parameters for Application 2: Continuous Blending of Two Covariance Functions<sup>a</sup>

Parameter	Value
<i>Trend Model of Log Conductivity</i>	
Type	linear
Equation	$E[Y(\mathbf{x})] = \beta_0 + \beta_1 x_1 + \beta_2 x_2$
Prior mean	
Intercept	$E[\beta_0] = \ln(10^{-4})$
$x_1$ component of gradient	$E[\beta_1] = 0$
$x_2$ component of gradient	$E[\beta_2] = 0$
Prior standard deviation	
Intercept	$\sigma_{\beta_0} = \ln(10)$
$x_1$ component of gradient	$\sigma_{\beta_1} = 0.01$
$x_2$ component of gradient	$\sigma_{\beta_2} = 0.01$
<i>Covariance of Random Log Conductivity Fluctuations</i>	
Covariance model 1	
Type	isotropic Gaussian
Variance	$\sigma_Y^2 = 0.5$
Correlation length	$\lambda = 2$ m
Covariance model 2	
Type	isotropic Gaussian
Variance	$\sigma_Y^2 = 1.0$
Correlation length	$\lambda = 10$ m
Covariance blending	
Type	linear blending in $x_2$
Scaling function for model 1	$A_1(\mathbf{x}) = \sqrt{1 - \frac{x_2}{L_2}}$
Scaling function for model 2	$A_2(\mathbf{x}) = \sqrt{\frac{x_2}{L_2}}$
<i>Measurements of Heads and Log Conductivities</i>	
Measurement locations	
General setup	regular grid
Longitudinal coordinates	$x_1 = 10$ m, 20 m, ..., 90 m
Transverse coordinate	$x_2 = 5$ m, 15 m, ..., 45 m
Standard deviation of measurement errors	
Type	uncorrelated, Gaussian
Log conductivity measurements	$\sigma_{meas,Y} = 1$
Head measurements	$\sigma_{meas,\phi} = 10^{-3}$ m

<sup>a</sup>Geometry of the domain, boundary conditions for flow, transport parameters, and locations of travel time observation are identical to application 1.

the travel time distribution, shown in Figure 3, plot A3, reflect these structures: we see large-scale variations in the flow net and large “fingers” in the travel time at the top part of the domain in contrast to small-scale variations at the bottom. The travel time distribution shows a particularly pronounced finger of high travel time values originating from a low-conductivity zone at  $x_1 \approx 50$  m,  $x_2 \approx 35$  m. This finger leads to the maximum in the travel time profile at the observation plane shown in Figure 4.

[49] Figure 3, plots B1–B3, shows the uniform prior mean of the log conductivity distribution, the resulting regular flow net and the uniformly increasing travel time distribution. The corresponding variance  $\sigma_{\tau|\beta}$  of travel time along the observation plane is plotted as dashed-dotted line in Figure 5. This line refers to the case of a perfectly known and uniform mean value of the log conductivity. Although the mean travel time is uniform over the cross-section, its variance exhibits a distinct trend. This is caused by the trend in the covariance function of log conductivities. At small  $x_2$  values, the smaller variance and integral scale of covariance function 1 dominate the uncertainty in travel time, whereas, at large  $x_2$

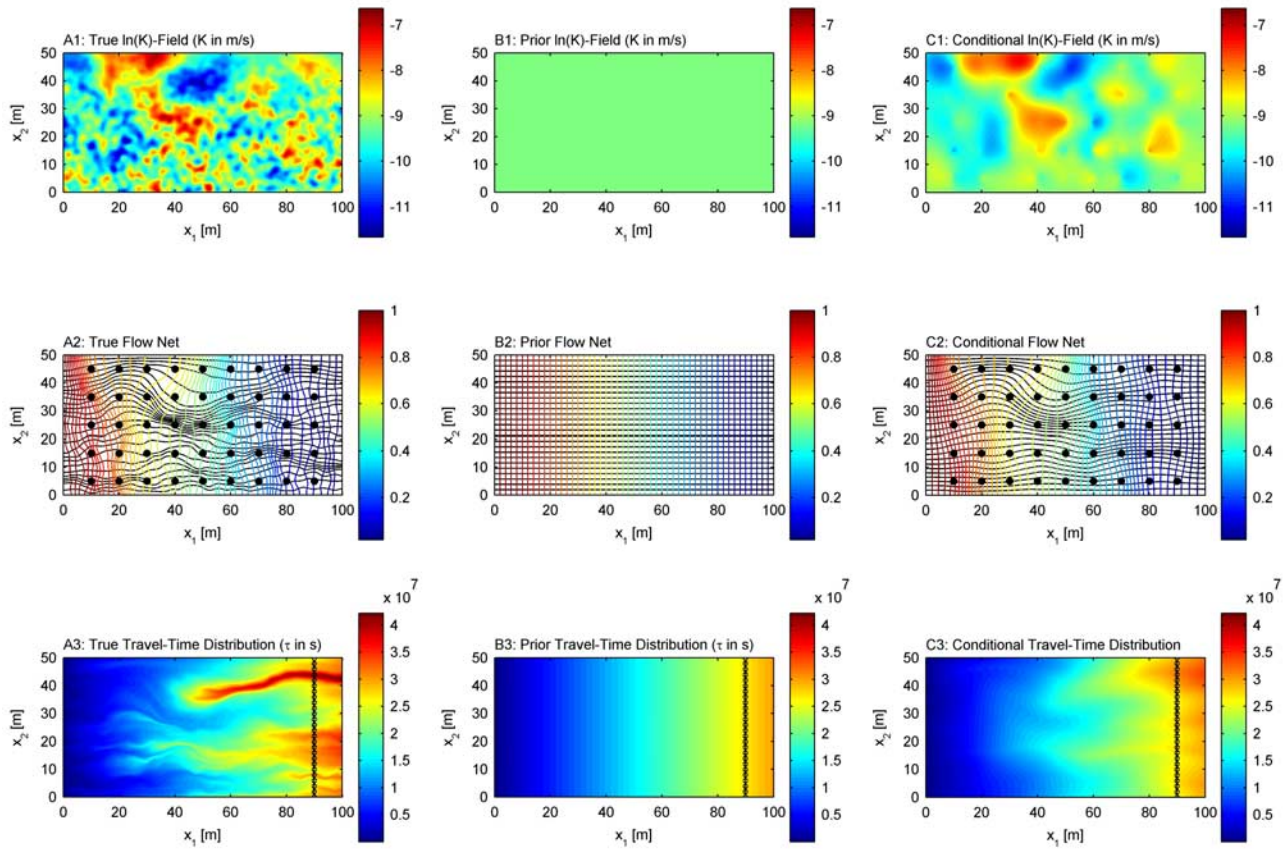


Figure 3. Application 2: Log conductivity fields, flow nets, and travel time distributions.

values, the larger variance and integral scale of covariance function 2 become effective.

[50] In the inverting procedure, we assume an uncertain mean log conductivity following a linear trend model. The standard deviation  $\sigma_{\beta_0}$  of the uniform part in the trend model reflects prior uncertainty in the conductivity by one order of magnitude. We believe that our choice of  $\sigma_{\beta_0}$  is a realistic

value for many situations in which the aquifer material is only characterized qualitatively. A priori, the linear trend coefficients are assumed zero with only a small uncertainty. The uncertainty in the mean log conductivity enhances the uncertainty in the travel time dramatically. The prior variance of travel time after marginalization,  $\sigma_{\tau}^2$ , is plotted in Figure 5 as a solid line. The spatial trend in the marginal

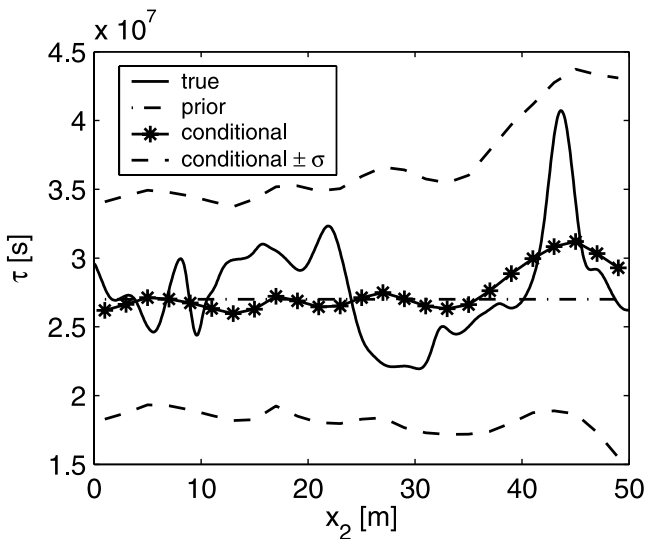


Figure 4. Application 2: Travel time distribution on the control plane.

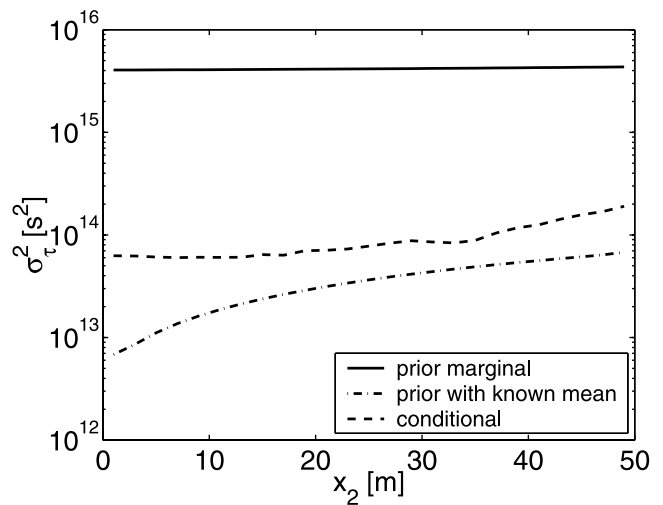


Figure 5. Application 2: First-order variance of travel time on the control plane.

variance  $\sigma_\tau^2$  is slightly enhanced in comparison to the case with known trend parameters,  $\sigma_{\tau|\beta}^2$ , although this is hardly visible in the logarithmic plot of Figure 5. In the given application, the highest contribution to the uncertainty in the travel time comes from the uncertainty in the uniform coefficient of the trend model.

[51] In Figure 3, plots A2 and C2, the locations of head and log conductivity measurements are marked by black dots. We assume a standard deviation of the head measurements of 1 mm and of the log conductivity measurements of one logarithmic unit. The rationale for these values is that heads can be measured fairly accurately, whereas the log conductivity measurements are typically indirect estimates, for instance derived from the grain-size distribution of the material obtained during drilling of the monitoring wells. The artificial measurements are the actual values plus artificially generated measurement errors. Figure 3, plot C1, shows the estimate of the log conductivity distribution derived by iterative cokriging using the measurements. The large-scale features of the log conductivity field are reproduced well. The small-scale fluctuations, dominating the bottom part of the domain, can hardly be recovered, simply because the characteristic length of these features is smaller than the distance between measurement points. Figure 3, plot C2, shows the conditional mean flow net. Again, large-scale features like the overall meandering of streamlines are recovered well whereas the small-scale fluctuations are smoothed out. In general, heads are reproduced better than velocities.

[52] Figure 3, plot C3, shows the mean conditional distribution of the travel time throughout the domain. In Figure 4 the mean conditional travel time along the observation plane is plotted as solid line supplemented with asterisks. Although the hydraulic heads of the measurements are met within the measurement error of 1 mm, the conditional mean of the travel time still differs significantly from the true values of the realization. The true values, however, fall within the error bound of  $E[\tau|Z^m] \pm \sigma_{\tau|Z^m}$ . The conditional variance  $\sigma_{\tau|Z^m}^2$  of the travel time given the head and log conductivity measurements is plotted in Figure 5 as a dashed line. Conditioning reduces the uncertainty in travel time. In inverting with uncertain trend parameters, however, it is important that the reference covariance is the marginal one, which accounts for the uncertainty of the trend parameters. In our application, the conditional variance of travel time,  $\sigma_{\tau|Z^m}^2$ , is even larger than the corresponding unconditional covariance  $\sigma_{\tau|\beta}^2$  for the case with perfectly known trend parameters. As has been emphasized by *Kitanidis* [1996], one needs to take into account the prior uncertainty in the mean when evaluating the conditional variance. In our inverting application, the conditional covariance  $\mathbf{Q}_{\mathbf{Y}\mathbf{Y}|Z^m}$  of the log conductivity values is the very basis of uncertainty propagation and must not be biased by “forgetting” the marginalization.

## 8. Discussion and Conclusions

[53] We have presented an efficient numerical method for evaluating the variance of travel time in formations with a nonstationary covariance function of the log conductivity field. In our applications, we considered  $1000 \times 500 = 5 \times 10^5$  log conductivity values. On a 2GHz Pentium IV computer, it took about seven minutes to compute the

sensitivity of a single travel time value with respect to all log conductivity values. Once the sensitivity matrix  $\mathbf{H}_\tau$  was computed, evaluating the covariance matrix of travel time observations  $\mathbf{Q}_{\tau\tau}$  took only a few additional minutes. In other words, our combination of methods makes it possible to compute travel time statistics for highly resolved nonstationary log conductivity fields within a reasonable time-frame and with reasonable requirements for computer memory. More realistic three-dimensional applications are merely a matter of numerical implementation.

[54] Our method requires that the log conductivity values are discretized on a regular grid. Otherwise, the stationary counterpart of the covariance function would not be discretized as a Toeplitz matrix, which is a prerequisite for embedding in a circulant matrix and subsequent multiplication by FFT techniques. Irregularly shaped domains could be accounted for by deactivating elements outside the domain, as is common in Finite Differences schemes. Local grid refinement in the simulation of flow and transport is possible as long as the conductivity is defined on the regular grid.

[55] We have covered four basic types of nonstationarity in the covariance function. The first one results from variance scaling of stationary covariance functions, and the second from combining several scaled functions. On the discretized level, the scaling can be expressed as a quadratic matrix-matrix multiplication. The third and fourth types of nonstationarity in the covariance function result from marginalization or conditioning. Here we consider the sum of a standard covariance matrix, which itself may not be of the Toeplitz type, and a quadratic matrix-matrix product with a center matrix that is typically much smaller than the covariance matrix. For all four types of nonstationary covariance function, we can save computational effort and memory in the uncertainty propagation when we choose the right order of performing the resulting matrix multiplications. Among the models for nonstationary media that we have not covered is the model of multimodal distributions resulting from zonal stationarity with uncertain distribution of the zones [see *Zhang*, 2002, sect. 2.3.3; *Rubin*, 2003, chap. 2.5].

[56] The matrix-based first-order second-moment (FOSM) method is subject to the limits of first-order stochastic analysis. Cases with high variance may be biased because of the nonlinear dependence of travel times  $\tau(\mathbf{x})$  on log conductivities  $Y(\mathbf{x}_1)$ . For nonstationary formations discretized by many log conductivity values, however, second-order corrections are not practical because the matrix of second derivatives, or Hessian,  $\partial^2\tau(\mathbf{x})/(\partial Y(\mathbf{x}_1)\partial Y(\mathbf{x}_2))$  of a single travel time value with respect to all log conductivity values has a size of  $n_y \times n_y$ , and requires the solution of  $\mathcal{O}(n_y)$  adjoint problems. For the domain sizes discussed in the present study, performing several thousand Monte Carlo simulations would be computationally less demanding than evaluating second-order correction terms.

[57] Our analysis is restricted to the variance of the mean travel time observed at defined observation points. We do not evaluate the expected spread of actual breakthrough curves at these points. *Cirpka and Kitanidis* [2000b] used the local second-central temporal moments to predict mixing-controlled reactive transport in heterogeneous domains, and *Vanderborgh and Vereecken* [2001] used it to estimate pore-scale dispersion coefficients from field measurements.

Thus extending existing methods to estimate the spread of point-related breakthrough curves in stationary flow fields to nonstationary ones would be valuable. We believe, however, that this goal is still beyond current capacities. In the Lagrangian method of *Zhang et al.* [2000] the expected spread of point-related breakthrough curves is zero because these authors neglected pore-scale dispersion altogether. In our framework, we could easily evaluate the zeroth-order second-central moments of breakthrough curves by solving an additional moment-generating equation. The result, however, would neglect the impact of unresolved spatial variability on the spread of local breakthrough curves. To predict how solutes actually mix in nonstationary formations, one would need to apply a second-order first-moment (SOFM) approach for the second-central temporal moment. The formalism can be written down easily. However, it requires the evaluation of the Hessian which is, as discussed above, computationally demanding.

### Appendix A: Derivation of Moment-Generating Equations

[58] In this appendix, we restate the derivation of the temporal moment-generating equations as given by *Cirpka and Kitanidis* [2000a]. The  $k$ -th temporal moment  $M_k(\mathbf{x})$  of the concentration  $c(\mathbf{x}, t)$  is defined as:

$$M_k(\mathbf{x}) = \int_0^\infty t^k c(\mathbf{x}, t) dt \quad (\text{A1})$$

We consider the advection-dispersion equation for an ideal tracer:

$$\frac{\partial c}{\partial t} + \frac{\mathbf{q}}{\theta} \cdot \nabla c - \nabla \cdot (\mathbf{D} \nabla c) = 0 \quad (\text{A2})$$

subject to the initial condition:

$$c(\mathbf{x}, t_0) = 0 \quad \forall \mathbf{x} \quad (\text{A3})$$

and the boundary conditions:

$$\begin{aligned} \mathbf{n} \cdot \left( \frac{\mathbf{q}}{\theta} c - \mathbf{D} \nabla c \right) &= \frac{\mathbf{n} \cdot \mathbf{q}}{\theta} \frac{\delta(t)m}{Q} && \text{on } \Gamma_{in} \\ \mathbf{n} \cdot (\mathbf{D} \nabla c) &= 0 && \text{on } \Gamma \setminus \Gamma_{in} \end{aligned} \quad (\text{A4})$$

We multiply equation (A2) by  $t^k$  and integrate over time,  $\int_0^\infty dt$ , to obtain:

$$\begin{aligned} &\int_0^\infty t^k \frac{\partial c}{\partial t} dt + \int_0^\infty t^k \frac{\mathbf{q}}{\theta} \cdot \nabla c dt - \int_0^\infty t^k \nabla \cdot (\mathbf{D} \nabla c) dt \\ &= - \int_0^\infty kt^{k-1} c dt \\ &\quad + [t^k c]_0^\infty + \frac{\mathbf{q}}{\theta} \cdot \nabla \left( \int_0^\infty t^k c dt \right) - \nabla \cdot \left( \mathbf{D} \nabla \left( \int_0^\infty t^k c dt \right) \right) \\ &= 0 \Rightarrow \frac{\mathbf{q}}{\theta} \cdot \nabla M_k - \nabla \cdot (\mathbf{D} \nabla M_k) = k M_{k-1} \end{aligned} \quad (\text{A5})$$

in which we have applied integration by parts to the storage term, considered that the initial concentration and the

concentration at the infinite time limit equal zero, and exchanged the order of spatial differentiation and temporal integration in the advective-dispersive terms. We repeat the same procedure with the boundary conditions, equation (A4):

$$\begin{aligned} &\int_0^\infty t^k \mathbf{n} \cdot \left( \frac{\mathbf{q}}{\theta} c - \mathbf{D} \nabla c \right) dt = \int_0^\infty t^k \frac{\mathbf{n} \cdot \mathbf{q}}{\theta} \delta(t) dt \quad \text{on } \Gamma_{in} \\ \Rightarrow \mathbf{n} \cdot \left( \frac{\mathbf{q}}{\theta} \int_0^\infty t^k c dt - \mathbf{D} \nabla \left( \int_0^\infty t^k c dt \right) \right) &= \begin{cases} \frac{\mathbf{n} \cdot \mathbf{q}}{\theta} \frac{m}{Q} & \text{for } k = 0 \\ 0 & \text{for } k > 0 \end{cases} \\ \Rightarrow \mathbf{n} \cdot \left( \frac{\mathbf{q}}{\theta} M_k - \mathbf{D} \nabla M_k \right) &= \begin{cases} \frac{\mathbf{n} \cdot \mathbf{q}}{\theta} \frac{m}{Q} & \text{for } k = 0 \\ 0 & \text{for } k > 0 \end{cases} \end{aligned} \quad (\text{A6})$$

and analogously:

$$\begin{aligned} &\int_0^\infty t^k \mathbf{n} \cdot (\mathbf{D} \nabla c) dt = 0 \quad \Gamma \setminus \Gamma_{in} \\ \Rightarrow \mathbf{n} \cdot (\mathbf{D} \nabla M_k) &= 0 \quad \Gamma \setminus \Gamma_{in} \end{aligned} \quad (\text{A7})$$

[59] Equation (A5) is a steady state transport equation with a distributed source term of  $kM_{k-1}$ . For the zeroth moment  $M_0$ , the source term is zero. Since the input of the zeroth moment is distributed uniformly over the inflow boundary, equation (A6),  $M_0$  is uniform over the entire domain,  $M_0 = m/Q \forall \mathbf{x}$ . For a nonuniform injection concentration  $c_{in}$  in equation (4), the zeroth moment would become nonuniform within the domain.

[60] The mean travel time is defined as the first temporal moment  $M_1$  normalized by the zeroth moment  $M_0$ :

$$\tau(\mathbf{x}) = \frac{M_1(\mathbf{x})}{M_0(\mathbf{x})} \quad (\text{A8})$$

[61] Because the zeroth moment  $M_0$  is uniform, we can bring the normalization with  $M_0$  into the differential operators of equation (A5). Normalizing the right-hand side of equation (A5) for  $k = 1$  yields a source term of unity throughout the domain. Thus we arrive at the steady state transport equation for the mean travel time  $\tau$  given by equation (6) subject to the boundary conditions given by equation (7).

### Appendix B: Derivation of Adjoint-State Equations

[62] The principles of the continuous adjoint-state method have been explained by *Sun and Yeh* [1990]. *Cirpka and Kitanidis* [2000a] have given the expressions for the temporal-moment generating equations discussed in Appendix A. In this appendix, we repeat the most important steps of the derivation. For brevity, we will not discuss the boundary integrals. For the derivation of the complete set of equations including the boundary conditions, please refer to *Cirpka and Kitanidis* [2000a].

[63] The starting points are the first-order expansions in the log conductivity of the groundwater flow equation, equation (1):

$$\nabla \cdot (K_g \nabla \phi' + K_g \nabla \phi^{(0)} Y') = 0 \quad (\text{B1})$$

and the transport equation for the travel time, equation (6):

$$-\frac{K_g}{\theta} \nabla \tau^{(0)} \cdot \nabla \phi' - \frac{K_g}{\theta} \nabla \tau^{(0)} \cdot \nabla \phi^{(0)} Y' - \frac{K_g}{\theta} \nabla \phi^{(0)} \cdot \nabla \tau' - \nabla \cdot (\mathbf{D} \nabla \tau') = 0 \quad (\text{B2})$$

Here primed quantities are first-order perturbations, quantities with the superscript (0) are zeroth-order expected values, and  $K_g = \exp(Y^{(0)})$  is the geometric mean of the conductivity which may be a function of space. Note that the dispersion tensor  $\mathbf{D}$  is assumed deterministic.

[64] Now we consider a weak form of equation (B1) by multiplying it with a test function  $\psi_{\phi\tau}$  and integrating over the domain. We apply Green's theorem sufficiently often so that all primed quantities appear as a derivative-free factor within the integral:

$$\int_{\Omega} \nabla \cdot (K_g \nabla \psi_{\phi\tau}) \phi' d\mathbf{x} - \int_{\Omega} K_g \nabla \phi^{(0)} \cdot \nabla \psi_{\phi\tau} Y' d\mathbf{x} + B.T. = 0 \quad (\text{B3})$$

$B.T.$  denotes the boundary integrals appearing from the application of Green's theorem.

[65] We also consider a weak form of equation (B2) by multiplying it with a different test function  $\psi_{\tau}$ , integrating over the domain, and applying Green's theorem:

$$\begin{aligned} \int_{\Omega} \nabla \cdot \left( \frac{K_g}{\theta} \nabla \tau^{(0)} \psi_{\tau} \right) \phi' d\mathbf{x} - \int_{\Omega} \frac{K_g}{\theta} \nabla \tau^{(0)} \cdot \nabla \phi^{(0)} \psi_{\tau} Y' d\mathbf{x} - \int_{\Omega} \frac{\mathbf{q}^{(0)}}{\theta} \cdot \nabla \psi_{\tau} \tau' d\mathbf{x} - \int_{\Omega} \nabla \cdot (\mathbf{D} \nabla \psi_{\tau}) \tau' d\mathbf{x} + B.T. = 0 \end{aligned} \quad (\text{B4})$$

In addition, a perturbation  $\tau'(\mathbf{x}_{0,\tau})$  of the travel time at the measurement location  $\mathbf{x}_{0,\tau}$  may be expressed by the following integral:

$$\tau'(\mathbf{x}_{0,\tau}) = \int_{\Omega} \delta(\mathbf{x}_{0,\tau}) \tau' d\mathbf{x} \quad (\text{B5})$$

Adding equations (B3) and (B4) to equation (B5) yields:

$$\begin{aligned} \tau'(\mathbf{x}_{0,\tau}) = \int_{\Omega} \left( \nabla \cdot (K_g \nabla \psi_{\phi\tau}) + \nabla \cdot \left( \frac{K_g}{\theta} \nabla \tau^{(0)} \psi_{\tau} \right) \right) \phi' d\mathbf{x} \\ - \int_{\Omega} \left( K_g \nabla \phi^{(0)} \cdot \nabla \psi_{\phi\tau} + \frac{K_g}{\theta} \nabla \tau^{(0)} \cdot \nabla \phi^{(0)} \psi_{\tau} \right) Y' d\mathbf{x} \\ - \int_{\Omega} \left( \frac{\mathbf{q}^{(0)}}{\theta} \cdot \nabla \psi_{\tau} + \nabla \cdot (\mathbf{D} \nabla \psi_{\tau}) - \delta(\mathbf{x}_{0,\tau}) \right) \tau' d\mathbf{x} + B.T. \end{aligned} \quad (\text{B6})$$

[66] Obviously, if we choose the test functions  $\psi_{\tau}$  and  $\psi_{\phi\tau}$  to meet equations (14) and (17), the integrals containing the perturbations of the heads  $\phi'$  and of the travel time  $\tau'$  vanish. The remaining expression relates the perturbation of the travel time  $\tau'(\mathbf{x}_{0,\tau})$  at location  $\mathbf{x}_{0,\tau}$  to the field of log conductivity fluctuations  $Y'(\mathbf{x})$ . Discretizing the log conductivity field by a set of piecewise constant values  $Y_{\lambda}$  and replacing  $\tau'(\mathbf{x}_{0,\tau})/Y'_{\lambda}$  by  $\partial\tau(\mathbf{x}_{0,\tau})/\partial Y_{\lambda}$  yields the sensitivity given in equation (20). The test functions are now called adjoint states, and their partial differential equations are known as adjoint-state equations. The boundary conditions given in section 3 are derived from the boundary conditions of the perturbed equations and the boundary integrals due to the application of Green's theorem [Cirpka and Kitanidis, 2000a].

[67] **Acknowledgments.** This study was funded by the Deutsche Forschungsgemeinschaft within the Emmy Noether program under grant Ci 26/3-4.

## References

- Brooks, A. N., and T. J. R. Hughes (1982), Streamline upwind/Petrov-Galerkin formulations for convection dominated flows with particular emphasis on the incompressible Navier-Stokes equations, *Comput. Methods Appl. Mech. Eng.*, *32*, 199–259.
- Cirpka, O. A., and P. K. Kitanidis (2000a), Sensitivities of temporal moments calculated by the adjoint-state method and joint inverting of head and tracer data, *Adv. Water Resour.*, *24*, 89–103.
- Cirpka, O. A., and P. K. Kitanidis (2000b), An advective-dispersive streamline approach for the transfer of conservative tracer data to reactive transport, *Water Resour. Res.*, *36*, 1209–1220.
- Cvetkovic, V. D., A. M. Shapiro, and G. Dagan (1992), A solute flux approach in transport in heterogeneous formations: 2. Uncertainty analysis, *Water Resour. Res.*, *28*, 1377–1388.
- Dagan, G., V. D. Cvetkovic, and A. Shapiro (1992), A solute flux approach in transport in heterogeneous formations: 1. The general framework, *Water Resour. Res.*, *28*, 1369–1376.
- Dettinger, M., and J. Wilson (1981), First-order analysis of uncertainty in numerical models of groundwater flow: 1. Mathematical derivation, *Water Resour. Res.*, *17*, 149–161.
- Dietrich, C., and G. Newsam (1997), Fast and exact simulation of stationary Gaussian processes through circulant embedding of the covariance matrix, *SIAM J. Sci. Comput.*, *18*, 1088–1107.
- Fiori, A., P. Indelman, and G. Dagan (1998), Correlation structure of flow variables for steady flow towards a well with application to highly anisotropic heterogeneous formations, *Water Resour. Res.*, *34*, 699–708.
- Golub, G., and C. V. Loan (1996), *Matrix Computations*, 3rd ed., Johns Hopkins Univ. Press, Baltimore, Md.
- Harvey, C. F., and S. M. Gorelick (1995), Temporal moment-generating equations: Modeling transport and mass-transfer in heterogeneous aquifers, *Water Resour. Res.*, *31*, 1895–1911.
- Indelman, P., and Y. Rubin (1995), Flow in heterogeneous media displaying a linear trend in the log conductivity, *Water Resour. Res.*, *31*, 1257–1265.
- James, A. I., W. D. Graham, K. Hatfield, P. S. C. Rao, and M. D. Annable (2000), Estimation of spatially variable residual nonaqueous phase liquid saturations in nonuniform flow fields using partitioning tracer data, *Water Resour. Res.*, *36*, 999–1012.
- Kitanidis, P. K. (1995), Quasi-linear geostatistical theory for inverting, *Water Resour. Res.*, *31*, 2411–2419.
- Kitanidis, P. K. (1996), On the geostatistical approach to the inverse problem, *Adv. Water Resour.*, *19*, 333–342.
- LaVenue, M., R. W. Andrews, and B. S. RamaoRao (1989), Groundwater travel time uncertainty analysis using sensitivity derivatives, *Water Resour. Res.*, *25*, 1551–1566.
- Li, S.-G., and D. McLaughlin (1995), Using the nonstationary spectral method to analyze flow through heterogeneous trending media, *Water Resour. Res.*, *31*, 541–551.
- Nowak, W., S. Tenkleve, and O. Cirpka (2003), Efficient computation of linearized cross-covariance and auto-covariance matrices of interdependent quantities, *Math. Geol.*, *35*, 53–66.
- Rubin, Y. (2003), *Applied Stochastic Hydrogeology*, Oxford Univ. Press, New York.
- Rubin, Y., and A. Bellin (1994), The effects of recharge on flow nonuniformity and macrodispersion, *Water Resour. Res.*, *30*, 939–948.

- Shapiro, A. M., and V. D. Cvetkovic (1988), Stochastic analysis of solute arrival time in heterogeneous porous media, *Water Resour. Res.*, *24*, 1711–1718.
- Stüben, K. (2001), A review of algebraic multigrid, *J. Comput. Appl. Math.*, *128*, 281–309.
- Sun, N. Z., and W. W.-G. Yeh (1990), Coupled inverse problems in groundwater modeling: 1. Sensitivity analysis and parameter identification, *Water Resour. Res.*, *26*, 2507–2525.
- Townley, L. R., and J. L. Wilson (1985), Computationally efficient algorithms for parameter estimation and uncertainty propagation in numerical models of groundwater flow, *Water Resour. Res.*, *21*, 1851–1860.
- Vanderborght, J., and H. Vereecken (2001), Analyses of locally measured bromide breakthrough curves from a natural gradient tracer experiment at Krauthausen, *J. Contam. Hydrol.*, *48*, 23–43.
- Zhang, D. (1998), Numerical solutions to statistical moment equations of groundwater flow in nonstationary, bounded, heterogeneous media, *Water Resour. Res.*, *34*, 529–538.
- Zhang, D. (2002), *Stochastic Methods for Flow in Porous Media*, Academic, San Diego, Calif.
- Zhang, D., R. Andricevic, A. Y. Sun, X. Hu, and G. He (2000), Solute flux approach to transport through spatially nonstationary flow in porous media, *Water Resour. Res.*, *36*, 2107–2120.

---

O. A. Cirpka and W. Nowak, Institut für Wasserbau, Universität Stuttgart, Pfaffenwaldring 61, 70550 Stuttgart, Germany. (olaf.cirpka@iws.uni-stuttgart.de; wolfgang.nowak@iws.uni-stuttgart.de)